Biochimica et Biophysica Acta 1857 (2016) 1925–1934

Contents lists available at ScienceDirect

Biochimica et Biophysica Acta

journal homepage: www.elsevier.com/locate/bbabio

On the mechanism of ubiquinone mediated photocurrent generation by a reaction center based photocathode

Vincent M. Friebe [a,1], David J.K. Swainsbury [b,1,2], Paul K. Fyfe [b,3], Wessel van der Heijden [a], Michael R. Jones [b], Raoul N. Frese [a,*]

[a] Department of Physics and Astronomy, LaserLaB Amsterdam, VU University Amsterdam, De Boelelaan 1081, Amsterdam 1081, HV, The Netherlands
[b] School of Biochemistry, Biomedical Sciences Building, University of Bristol, University Walk, Bristol BS8 1TD, United Kingdom

ARTICLE INFO

Article history:
Received 30 June 2016
Received in revised form 31 August 2016
Accepted 24 September 2016
Available online 28 September 2016

Keywords:
Biosolar cells
Bio-photovoltaics
Photoelectrochemistry
Photosynthesis
Biosensors
Bioelectronics

ABSTRACT

Upon photoexcitation, the reaction center (RC) pigment-proteins that facilitate natural photosynthesis achieve a metastable separation of electrical charge among the embedded cofactors. Because of the high quantum efficiency of this process, there is a growing interest in their incorporation into biohybrid materials for solar energy conversion, bioelectronics and biosensing. Multiple bioelectrochemical studies have shown that reaction centers from various photosynthetic organisms can be interfaced with diverse electrode materials for the generation of photocurrents, but many mechanistic aspects of native protein functionality in a non-native environment is unknown. In vivo, RC's catalyse ubiquinone-10 reduction, protonation and exchange with other lipid phase ubiquinone-10s via protein-controlled spatial orientation and protein rearrangement. In contrast, the mechanism of ubiquinone-0 reduction, used to facilitate fast RC turnover in an aqueous photoelectrochemical cell (PEC), may not proceed via the same pathway as the native cofactor.

In this report we show truncation of the native isoprene tail results in larger RC turnover rates in a PEC despite the removal of the tail's purported role of ubiquinone headgroup orientation and binding. Through the use of reaction centers with single or double mutations, we also show the extent to which two-electron/two-proton ubiquinone chemistry that operates in vivo also underpins the ubiquinone-0 reduction by surface-adsorbed RCs in a PEC. This reveals that only the ubiquinone headgroup is critical to the fast turnover of the RC in a PEC and provides insight into design principles for the development of new biophotovoltaic cells and biosensors.

1. Introduction

Most of the biosphere is powered by sunlight through processes of photochemical charge separation that take place in reaction centre (RC) pigment-protein complexes. Although they show variety in composition, structure and detailed mechanism, RCs from different organisms have the common attribute of displaying a very high quantum yield for solar energy conversion, defined as charges separated per photon absorbed [1]. This is achieved through a multi-step membrane-spanning electron transfer that stabilizes the photo-induced charge-separated state for hundreds of milliseconds [2,3]. This provides sufficient time for diffusional processes to remove electrons from the "negative terminal" of the RC and donate electrons to the "positive terminal", resetting the RC for the next turnover. Developments in our understanding of RC mechanism have influenced the design of new synthetic materials for solar energy conversion, and there is interest in the hybridization of both natural and engineered RC proteins with man-made materials for applications in photovoltaics [4–9], biosensing [10,11] and molecular electronics [12,13].

The principle that a naturally photovoltaic pigment-protein can generate a photocurrent if interfaced with an electrode was established decades ago [14], but recent years have seen an acceleration of interest in this aspect of solar energy conversion. Particular attention has been paid to the Photosystem I complex from oxygenic phototrophs [15–17] and both the RC and RC/light harvesting complexes from anoxygenic purple photosynthetic bacteria such as *Rhodobacter* (*Rba.*) *sphaeroides* [4–8,10,18–23]. Major preoccupations of this work have been the development of strategies for effective interfacing of the positive and negative terminals of the photovoltaic protein to the working and counter electrode, either through direct binding or the use of diffusional mediators [4–8,16–27]. In the case of RC's from purple bacteria a particularly effective strategy has been to use analogues of the natural electron donor and electron acceptor, cytochrome (cyt) c_2 and ubiquinone-10 (UQ_{10}), to connect the photovoltaic protein to the two electrodes [18,20,22,27–29]. At the positive terminal, cyt c_2, or more often the commercially-available mitochondrial equivalent cyt *c*, has

* Corresponding author.
E-mail address: r.n.frese@vu.nl (R.N. Frese).
[1] Authors contributed equally.
[2] Present address: Department of Molecular Biology and Biotechnology, University of Sheffield, Sheffield S10 2TN, UK.
[3] Present address: Division of Biological Chemistry & Drug Discovery, School of Life Sciences, University of Dundee, Dundee DD1 5EH, Scotland, UK.

http://dx.doi.org/10.1016/j.bbabio.2016.09.011
0005-2728/

been used to "wire" the transfer of electrons from the working electrode to an RC protein adhered via the natural electrostatic protein-protein interactions [18,27–29]. The same strategy has also been used for the larger complex in which the RC is surrounded by a light-harvesting 1 antenna protein (termed the RC-LH1 complex) [5,7]. At the negative terminal, short-chain water-soluble analogues of the natural UQ_{10}, such as ubiquinone-2 (UQ_2) [7,22,26,28,29] or ubiquinone-0 (UQ_0) [5,10,19], have been used to connect electron flow through the RC or RC-LH1 complex to the counter electrode.

The use of a natural protein as the photoactive element in a biophotovoltaic cell opens up the prospect of atomic-scale engineering of its structure to introduce desirable features such as redox engineering for larger open circuit voltage and protein-substrate self-assembly for higher current densities. Progress in this area requires a better understanding of precisely how a RC protein interacts physically and electrically with both the working and counter electrodes, and the extent to which natural photosynthetic mechanisms still operate when the protein is interfaced with synthetic materials.

In the *Rba. sphaeroides* RC (Fig. 1), photochemical charge separation takes place between a pair of excitonically-coupled bacteriochlorophyll molecules (P) near the periplasmic side of the photosynthetic membrane and a tightly-bound UQ_{10} (Q_A) near the cytoplasmic side, forming the radical pair $P^+Q_A^-$ [2,30]. Q_A acts as a single electron relay, passing the electron laterally in the membrane to a pseudosymmetrically-located UQ_{10} bound at the Q_B site, forming $P^+Q_B^-$ [31,32]. P^+ is re-reduced by a molecule of cyt c_2, resetting the RC for a second membrane-spanning electron transfer to form $P^+Q_A^-Q_B^-$. Subsequent double reduction of Q_B is coordinated with double protonation [31,32], and the ubiquinol (UQH_2) formed dissociates into the intramembrane phase to be replaced by a new molecule of UQ_{10}. In the native membrane the coordinated reduction and protonation of UQ_{10} is required to couple light powered electron flow to proton translocation across the membrane to form a proton motive force, but in a biophotovoltaic cell this complexity is not required. The diverse natural roles played by ubiquinone as a one electron relay in the Q_A site, a two-electron/two-proton acceptor at the Q_B site, and as a diffusional electron carrier have been previously characterized in solution via spectroscopic techniques [33] (Fig. 1).

In contrast, we employ electrochemical techniques to probe the diverse roles of the ubiquinones with relevance to the operation of a biophotovoltaic cell. We do so by measuring the photocurrents generated by electrode-bound RCs with mutations that block specific quinone-mediated electron or proton transfer steps within the RC, and by examining how isoprenoid "tail" length affects the capacity of ubiquinone to mediate diffusional charge transfer between electrodes. With recent large gains in photocurrent magnitude [4,5,7] and mounting interest in this field, this work provides insight into design principles for the development of more effective biophotovoltaic cells and biosensors.

2. Results

2.1. Structural characterization of the engineered RCs

Two engineered RCs were used to investigate how interruption of double reduction and double protonation of the dissociable Q_B ubiquinone would affect photocurrent generation by the RC. The first of these had a Trp substitution at Glu L212, a functionally important residue in the L-polypeptide that forms part of the Q_B binding pocket (mutation denoted EL212W). This residue is structurally equivalent to Ala M248 that

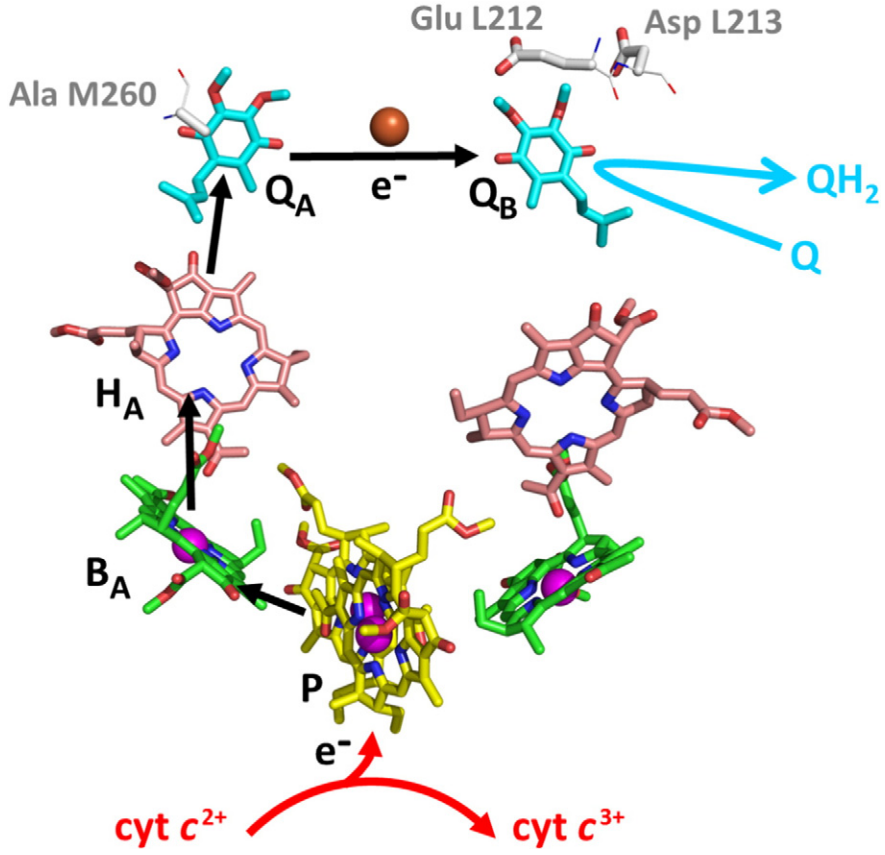

Fig. 1. Cofactor structure and electron transfer pathway in the RC. Charge separation (black arrows) takes place between the P BChl dimer (yellow carbons) and the Q_A UQ_{10} (cyan carbons) via a monomeric BChl (B_A — green carbons) and bacteriopheophytin (H_A — pink carbons). Q_A transfers the electron to the dissociable Q_B UQ_{10} (cyan carbons) whilst P^+ is reduced by cyt *c* (red arrows). After two membrane-spanning electron transfers the doubly reduced and doubly protonated Q_B ubiquinol dissociates and is replaced by ubiquinone (cyan arrow). The locations of the three mutated residues are shown in light-grey with backbone atoms shown as lines. Other atom colours are red — oxygen, blue — nitrogen, magenta spheres — magnesium, brown sphere — iron.

lines the Q_A binding pocket formed by the pseudosymmetrical M-polypeptide. Previous X-ray crystallography and functional studies have shown that substitution of Ala M248 for a much larger Trp residue results in steric exclusion of the Q_A ubiquinone from its binding pocket [34,35]. The EL212W mutation was therefore introduced with a view to blocking access of ubiquinone to the Q_B site. In addition, it has been reported that Glu L212 is responsible for delivery of the second proton to the Q_B ubiquinone [31,32,34,36,37] and so its replacement will prevent formation of QH_2 should quinone binding not be blocked by the Ala to Trp mutation.

The second engineered RC had Ala replacements of Glu L212 and the neighbouring Asp L213 (denoted EL212A/DL213A), mutations first constructed by Hanson and co-workers [37,38]. As a pair, residues Glu L212 and Asp L213 are structurally equivalent to residues Ala M248 and Ala M249 in the Q_A pocket and so this double mutation renders the Q_B pocket more "Q_A-like". Double replacement of Glu L212 and Asp L213 to Ala is known to block proton-coupled electron transfer after delivery of the first electron to ubiquinone at the Q_B site by preventing the transfer of both protons to the ubiquinone within the Q_B pocket [39,40] (for reviews see [32,41,42]).

The single and double mutations were constructed as described in Materials and Methods. Neither affected the absorbance spectrum of the RC bacteriochlorins and carotenoid (data not shown) or the stability of the RC during detergent extraction and purification. The protein structural changes accompanying these mutations, including the effect on binding of ubiquinone into the Q_B pocket, were investigated by X-ray crystallography.

2.1.1. Q_B binding site blocking mutant RC EL212W

An X-ray crystal structure was determined for the EL212W RC to a resolution of 2.4 Å, as described in Materials and Methods. Comparison with the X-ray crystal structure of the wild-type (WT) complex (Fig. 2a) revealed that the introduced Trp side chain (yellow carbons) occupied space normally occupied by the Glu side chain (cyan carbons) and nearby water molecules, but did not prevent binding of ubiquinone into the Q_B site (yellow carbons). Four water molecules modelled in the Q_B site of the WT RC (shown as teal semi-transparent spheres in Fig. 2a) were not resolved in the structure of the EL212W RC. The presence of the second water from the bottom in Fig. 2a was directly precluded by the Trp side chain, and electron density attributable to the three connected water molecules was not present. There was some hint of concerted movement of the head-group of the Q_B ubiquinone away from the mutation site, by between 0.3 and 0.5 Å (left and down in Fig. 2a). Although such a small structural change was close to the coordinate error for structures at this resolution, it was required to prevent a steric clash between one of the carbons of the Q_B headgroup and the new Trp side chain (the closest atom-to-atom approach between the two was 3.1 Å). These changes of structure aside, the Glu to Trp substitution did not affect the general structure of the RC in the immediate vicinity of the Q_B site or beyond.

2.1.2. Q_B protonation blocking mutant RC EL212A/DL213A (dAla)

An X-ray crystal structure for the double alanine EL212A/DL213A RC was previously determined to a resolution of 3.1 Å by Pokkuluri and coworkers [40]. In addition to the double residue substitution, this structure showed shifts in position of sections of backbone adjacent to the Q_B site. This encompassed amino acids L207-L227, with the strongest shifts being seen for amino acids L207-213 (~0.5 Å) and L223-L227 (~0.3–0.7 Å). There were also wider-spread small shifts in regions surrounding this, the net result being a small expansion of the Q_B cavity as a result of replacement of Glu L212 and Asp L213 by smaller Ala residues.

In the present work an X-ray crystal structure of a RC carrying this double mutation was determined to a resolution of 2.5 Å. Replacement of Glu L212 and Asp L213 by Ala did not induce any major changes in the structure of the Q_B binding pocket or significant changes in the detailed

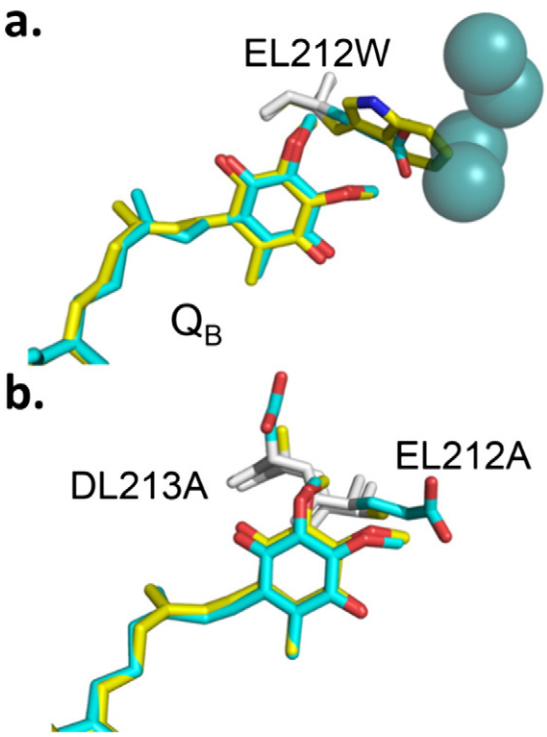

Fig. 2. Structural analysis of the EL212W and EL212A/DL213A RCs. a) Alignment of the X-ray crystal structures of the WT RC (cyan carbons) and EL212W RC (yellow carbons), showing four water molecules present in the Q_B pocket of the WT RC as semi-transparent teal spheres. b) Alignment of the X-ray crystal structures of the WT RC (cyan carbons) and EL212A/DL213A RC (yellow carbons). In both panels backbone atoms are shown in white, side chain or ubiquinone oxygens in red and side chain nitrogens in blue.

conformation of the Q_B ubiquinone (Fig. 2b). The small (0.5–0.7 Å) shifts in the positions of backbone and side chain atoms affecting amino acids L207-L213 and L223-227 described above were also seen in this new, higher-resolution X-ray crystal structure; in Fig. 2b this small expansion of the Q_B pocket can be seen as a lateral shift of the backbone atoms of amino acids L212 and L213 from left (WT) to right (mutant). These changes aside the structure of the EL212A/DL213A RC was well preserved, with clear occupancy of the Q_B site by ubiquinone.

It should be noted that, for the purposes of a parallel research project (Fyfe, P.K. and Jones, M.R., unpublished), the RC used to determine the structural consequences of the EL212A/DL213A mutations contained a third mutation of Leu M215 to Ala in the RC Q_A site. This third mutation also produced no significant change in the structure of the RC outside the immediate vicinity of the Q_A site. This additional mutation was not present in the EL212A/DL213A RC used for all other measurements described below, and for convenience this RC is referred to as "dAla" in the following.

2.2. Functional characterization of the engineered RCs

The effects of mutation on the reduction of Q_B were monitored through recovery of photo-oxidation of P as a result of $P^+Q_A^-$ or $P^+Q_B^-$ recombination. In detergent-isolated WT RCs the recombination reaction $P^+Q_B^- \rightarrow PQ_B$ occurs with a time constant in the region of 1–2 s, whereas the recombination of $P^+Q_A^- \rightarrow PQ_A$ occurs with a time constant in the region of 100–200 ms [43]. As these two processes are reasonably kinetically distinct, in the WT RC they can be used as an approximate measure of occupancy of the Q_B site, on the premise that the yield of electron transfer from Q_A^- to Q_B is 100%. The kinetics of P^+Q^- charge recombination in isolated WT RCs were monitored through millisecond time scale recovery of P ground state absorbance at 865 nm. In the

absence of exogenous ubiquinone, measurements on WT RCs (Fig. 3, purple) revealed two recovery components with time constants of 1.2 s and 200 ms, and relative amplitudes of 81% and 18%, respectively (Table 2). These values corresponded well with typical data from the literature [43] and indicated that ~80% of WT RCs have their native Q_B intact after purification. In the presence of a ~20-fold excess of UQ_{10} (250 μM) or a ~75-fold excess of UQ_0 (1 mM) a complete loss of the faster recovery phase was observed (not shown) indicating the Q_B site could be functionally reconstituted with both the native UQ_{10} and isoprene tail truncated form UQ_0 (Table 2).

2.2.1. Q_B protonation blocking mutant RC dAla

The kinetics of charge recombination were markedly altered in purified dAla RCs, with a 52% contribution from a fast component and a second, very slow recovery component with a time constant of 22 s (Fig. 3, red). Hence replacement of Glu/Asp with Ala resulted in a significantly lower yield of Q_B^- than was the case for the WT RC and also very strongly slowed $P^+Q_B^-$ recombination. Also in contrast with data for the WT RC, full reduction of Q_B could not be reconstituted using either 1 mM UQ_0 (31% yield of Q_B^-) or 250 μM UQ_{10} (48% yield of Q_B^-) (Table 2). These findings were consistent with previous reports that double replacement of Glu L212 and Asp L213 with Ala [37] or Gln/Asn [31] stabilizes the Q_B^- semiquinone, strongly slows the rate of $P^+Q_B^-$ recombination, and weakens affinity for quinone binding leading to lowered levels of reconstitution [41], and we conclude that the reduced level of Q_B^- seen in the dAla RC was mainly due to lowered occupancy of the Q_B site by native UQ_{10} or added UQ_0.

2.2.2. Q_B binding site blocking mutant RC EL212W

Purified EL212W RCs displayed a single rapid phase of P^+ reduction with a time constant of 125 ms, consistent with 100% recombination from Q_A^- (Fig. 3, orange). This could either indicate an absence of native UQ_{10} binding at the Q_B site, or a shutting off of electron transfer from Q_A^- to Q_B due to destabilisation of Q_B^-. Given that electron density for Q_B was obtained in the X-ray crystal structure of the EL212W RC the first of these scenarios would seem implausible, but the X-ray data would not rule out that the Q_B site in the purified EL212W RC is partially occupied by UQ_{10} that cannot be reduced by Q_A^-. Interestingly, incubating EL212W RC with 250 μM UQ_{10} did not change the rate of charge recombination but incubation with 1 mM UQ_0 produced a slow, 4.4 s decay component with an amplitude of 13% (Table 2). A possible explanation is that, due to the lack of a tail, binding conformations and local interactions ofUQ_0 bound into the Q_B site may be less restricted allowing it to undergo reduction whereas UQ_{10} is not. Regardless of the correct interpretation of these data, it was possible to conclude that the EL212W mutation prevents formation of Q_B^- in the presence of UQ_{10}, and largely prevents its formation in the presence of UQ_0, although it is possible that the Q_B site was occupied with quinone.

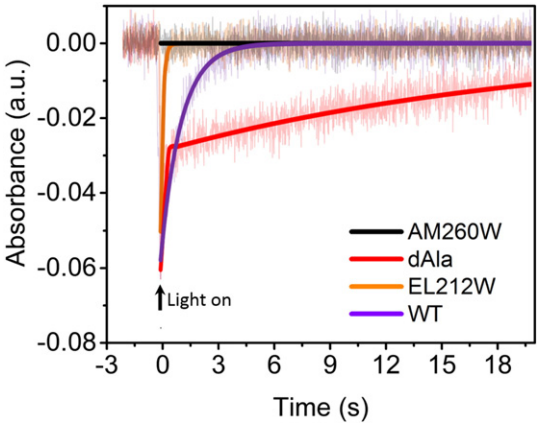

Fig. 3. P^+Q^- recombination kinetics at 865 nm in isolated RCs following flash excitation. Data (average of 8 repeat traces) are shown with faded lines and fits are overlaid with solid lines.

2.2.3. Q_A binding site blocking mutant RC AM260W

Recombination of P^+Q^- was also examined in a RC with replacement of Ala 260 in the M-polypeptide with Trp (AM26 0 W). This mutation causes the RC to assemble without a Q_A ubiquinone, halting charge separation at the $P^+H_A^-$ state. The AM260W RC has been characterized by a range of spectroscopic techniques [35,44,45], and a 2.1 Å resolution X-ray crystal structure has been determined that showed a lack of a ubiquinone at the Q_A site and a Q_B site occupied by UQ_{10} [36]. In the present study, photoexcitation of purified AM260W RCs failed to produce a change in 865 nm absorbance, indicating a lack of P^+ formation on a millisecond time scale (Fig. 3, black). This was consistent with the fact that the $P^+H_A^-$ state formed in Q_A-deficient RCs recombines in a few tens of nanoseconds [44] and so P oxidation is not detected on a millisecond time scale. This lack of a response was not changed if AM260W RCs were incubated in the presence of 250 μM UQ_{10}, but when the measurement was carried out in the presence of 1 mM UQ_0 a light induced bleach of P ground state absorbance was obtained with approximately one third of the amplitude of that of the same concentration of WT RCs (not shown). This P^+ signal decayed with time constants of 0.1 s (52% amplitude) and 2.6 s (48% amplitude) (Table 3), which implies the formation of approximately equal amounts of $P^+Q_A^-$ and $P^+Q_B^-$ in the subpopulation of RCs that had a UQ_0 at the Q_A site. This indicated that in the case where a UQ_0 was bound in the Q_A site, electron transfer to Q_B in these Q_A-reconstituted RCs proceeds with significantly reduced efficiency.

2.3. Choice of electrode surface for comparative measurements

The three engineered RCs described above were used to test the mechanism of photocurrent generation by comparison of the photocurrent densities obtained when each RC was interfaced with an electrode surface. In previous work it has been shown that RCs generate sizeable photocurrents when interfaced with an unfunctionalised planar gold electrode, using cyt *c* and UQ_0 as redox mediators [5,10,13,20]. However, one finding was that the absolute current density was variable from one coated electrode to the next under a given set of conditions, probably due to variations in loading of RCs on the electrode surface through drop casting. In an attempt to improve reproducibility, which is important for a comparative study, functionalization of the gold electrode surface was explored.

In the present study the working gold electrode was coated with a thin SAM formed from 4-mercaptopyridine (4-MP) [46]. This SAM could be applied through a simple 10 min incubation, as opposed to a 12–24 h process for other organo-sulfur compounds [47], and therefore did not significantly complicate electrode fabrication. RC deposition on SAM-coated electrodes was achieved by drop casting followed by careful rinsing, then incubation with 200 μM cyt *c* followed by further rinsing. Photocurrents from such assembled Au|4-MP|cyt *c*| WT RC electrodes were measured in a liquid three-electrode photoelectrochemical cell containing UQ_0 as the solution electron acceptor. Gold electrodes coated with a 4-MP SAM supported a consistently larger RC photocurrent (Fig. 4a, blue) when compared to otherwise equivalent bare gold electrodes (Fig. 4a, red), and improved the reproducibility of the photocurrent densities obtained (note the relative sizes of the errors in Fig. 4a, represented by the shaded areas).

To look at the source of the measured photocurrent and assess the structural integrity of the RC when deposited on the substrates, the external quantum efficiency (EQE) of the electrodes was calculated between 450 and 930 nm using monochromatic excitation, as previously described [5]. The EQE showed good agreement with the solution absorption spectrum of the RC (Fig. 4b), indicating that the RC had retained its native structure on both the bare gold and SAM covered electrode. As with the photocurrent density, the absolute magnitude

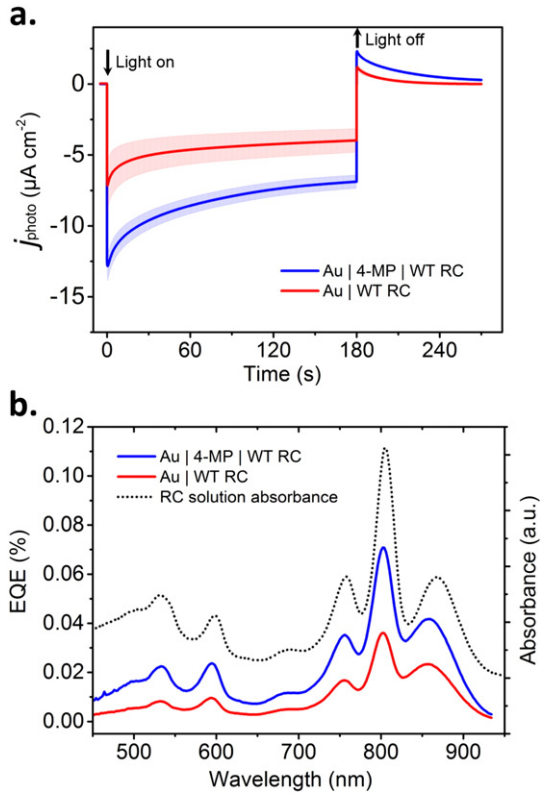

Fig. 4. Photocurrent response from working electrodes fabricated with WT RCs. a) Photocurrent density in response to 180 s of illumination (46 mW cm^{-2} LED at 870 nm) at a bias of −100 mV vs SCE. The shaded region represents one standard deviation, n = 4. b) Wavelength dependence of EQE compared with the RC absorbance spectrum (right axis, dotted black line, offset vertically for clarity).

of the EQE was proportionally higher on the Au|4-MP electrode relative to a bare gold electrode, probably due to a higher protein loading or a more optimal protein orientation on the electrode surface.

2.4. Suitability of different ubiquinones as redox mediator

To further explore parameters that influence photoelectrochemical cell performance, ubiquinones with tails formed from zero, one, two, four or ten isoprene units were compared as mediators of current flow to the counter electrode. RC photoelectrochemical cells were constructed with UQ_0 and UQ_1 at 500 μM and maximum achievable concentrations of 326 μM, 3.0 μM and 0.1 μM for UQ_2, UQ_4 and UQ_{10}, respectively. Upon illumination an initial peak photocurrent response was observed which decayed over a period of 3–4 min (Fig. 5). The maximum photocurrent was obtained with UQ_0, with an appreciable current also being obtained with UQ_1. Extending the length of the isoprenoid tail through two, four and ten isoprene units produced a decreased initial peak photocurrent, an increasingly rapid decay of the peak photocurrent, and a decreased steady state photocurrent. As the solubility of the quinone decreases dramatically with increasing tail length, we interpret these data to suggest that the concentration of mediator is the limiting factor and greatly outweighs the negative effect of reduced affinity for the Q_B pocket of non-native quinones, especially UQ_1 and UQ_0 [48]. This further suggests that diffusive electron flux to the counter electrode is a major limiting factor in steady-state photocurrent generation in these cells.

When WT RCs depleted of the native UQ_{10} at the Q_B site were used for such measurements no differences in peak or transient photocurrent were obtained with UQ_0 as the mediator compared to RCs with a normal complement of native UQ_{10} in the presence of bulk UQ_0 (data not shown). This suggests a mechanism where UQ_0 enters the buried Q_B site for reduction and protonation rather than a more complex

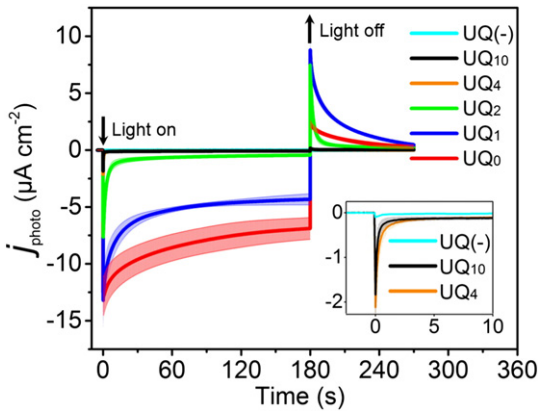

Fig. 5. Effect of ubiquinol isoprenoid tail length on photocurrent density from WT RCs. Photocurrents from Au|4-MP|cyt *c*|WT RC electrodes were measured for 180 s of illumination (45 mW cm^{-2} LED at 870 nm) at a bias of −100 mV vs SCE. The shaded region represents one standard deviation, n = 4. UQ(−) denotes no added ubiquinone.

mechanism where, for example, a native bound UQ_{10} at the Q_B site passes electrons to the water-soluble UQ_0.

2.5. Photochronoamperometry of engineered RCs

For comparative measurements of photocurrent generation, Au|4-MP|cyt *c*|RC working electrodes fabricated with WT or engineered RCs were immersed in buffer containing 500 μM UQ_0. With WT RCs (Fig. 6, purple) a peak cathodic photocurrent of 12.8 ± 1 μA cm^{-2} was observed which, based on an estimate of RC loading (See methods 6.8), corresponded to an apparent turnover rate of 12 ± 1 electrons s^{-1} RC^{-1} or the transit of one electron per 83 ms (see Materials and Methods for calculation). Under otherwise identical conditions, all three mutated RCs produced a strongly decreased mean peak photocurrent relative to that obtained for WT RCs, levels being 5%, 8% and 3% for the dAla, EL212W and AM260W RC, respectively (inset to Fig. 6 and Table 3).

For comparison, the effects of abolishing binding of ubiquinone at the Q_B site was determined through the addition of the tight-binding inhibitor stigmatellin [49]. This reduced photocurrent generation to 0.7% of the level seen with WT RCs (Fig. 6, green), demonstrating that most of the residual photocurrent seen in the three engineered RCs arose from a mechanism involving ubiquinone binding, reduction and exchange process at the Q_B site, rather than some other light-activated redox process.

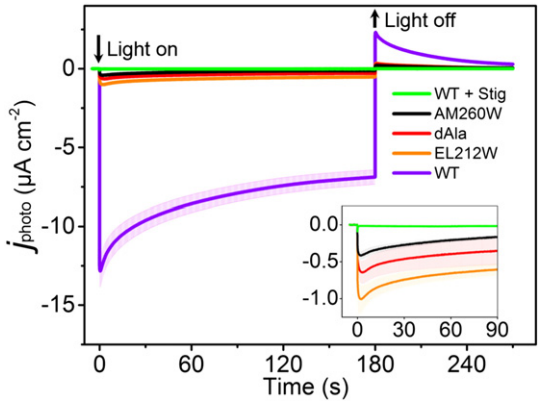

Fig. 6. Comparison of photocurrent response from working electrodes fabricated from WT and engineered RCs. Irradiance was for 180 s (45 mW cm^{-2} LED at 870 nm). Solutions contained 500 μM UQ_0, and were performed under −100 mV vs SCE. Error bars indicated standard deviation (n = 4).

3. Discussion

Although the in vivo mechanism by which the RC produces electrons via the double reduction and protonation of ubiquinone is well characterized, the precise mechanism of electron transport in this type of photoelectrochemical cell studied by ourselves and others has not previously been explored. In this work we employed site-directed mutants to systematically block electron transfer and protonation steps necessary to form the ubiquinol product.

Exclusion of UQ_{10} from the Q_A pocket through the AM260W mutation reduced the observed photocurrent by ~97% with 500 μM UQ_0 as the mediator, indicating that formation of the $P^+Q_A^-$ state is necessary for photocurrent generation. This mutation has been used by a number of groups to shut off electron transfer from H_A^- to Q_A in order to study primary charge separation without formation of long-lived radical pairs [50], $P^+H_A^-$ recombination [51], and the activation of inactive branch electron transfer [52–55]. In a recent report employing conductive atomic force microscopy on an orientated RC monolayer [13] it was shown that this mutation abolishes electron conduction across the RC under an applied bias, revealing that the strong functional asymmetry displayed by natural charge separation is retained when the RC is incorporated into an electrical circuit. A prediction of this finding is that the AM260W mutation should completely block photocurrent generation, but a residual current at ~3% of wild-type levels was routinely observed (Fig. 6, inset). Insight into the source of this small current came from measurements of P^+Q^- charge recombination, where incubation of AM260W RCs with 1 mM UQ_0 caused the appearance of a 865 nm absorbance change implying formation of a mixture of Q_A^- or Q_B^- in around one third of the RCs. This finding suggests that this Ala to Trp mutation does not absolutely block binding of ubiquinone-0 at the Q_A site, and that an impaired Q_A activity can be partially restored in the presence of a large (75-fold) molar excess of UQ_0 (but not the native UQ_{10}). The residual photocurrent seen for AM260W RCs can therefore be attributed to a low level of reconstitution of Q_A activity due to the presence of 500 μM UQ_0 as the mediator.

The remaining mutations affected two residues known to be important for operation of the Q_B catalytic site. The mechanism of proton-coupled electron transfer at this site is complex, and has been studied through a combination of spectroscopy, computation and site-directed mutagenesis (for reviews see [32,41,56]). The role of Asp L213 is delivery of the first proton to the Q_B semiquinone immediately preceding the second electron transfer. Residue Glu L212 is protonated following the first electron transfer, and its role is to be to deliver the second proton to the Q_B ubiquinone following delivery of the second electron. The double mutation EL212A/DL213A therefore blocks Q_B site function after the first electron transfer and the single EL212W mutation would be expected to block Q_B site function after the second electron transfer by preventing the second protonation.

Strongly attenuated photocurrents (see Table 3) were obtained with the EL212W and dAla RC despite the fact that the X-ray crystal structures showed that these mutations do not abolish binding of UQ_{10} at the Q_B site. The EL212W mutation prevented formation of Q_B^- in the presence of an excess of UQ_{10} and produced only 13% Q_B^- in the presence of UQ_0, and so the small photocurrent obtained with this RC at 7.8% of wild-type levels could be interpreted as simply reflecting reduced reduction of Q_B. The situation with the dAla mutation was more complex than this however, as up to a 48% yield of Q_B^- could be achieved in measurements of P^+Q^- recombination in this RC, but the measured photocurrent was only 5.0% of that obtained with the WT RC. The low photocurrent here is likely also a consequence of the inability of Q_B^- to undergo protonation and further reduction due to substitution of Glu L212 and Asp L213, rendering it incapable of forming the reduced QH_2 product which can then dissociate and exchange for an oxidized UQ.

An additional marked feature of the data collected on the dAla RC was the very long lifetime of the slow phase of P^+Q^- recombination, determined to be ~20 s with UQ_{10} and ~11 s with UQ_0 compared to ~1.2 s for the WT RC. This long lifetime indicates stabilization of Q_B^- by this double mutation, in accord with previous observations [35]. In a photoelectrochemical cell, with a mechanism for effective reduction of P^+ by the working electrode using cyt *c* as a "wire", such stabilization would be expected to result in photoaccumulation of RCs initially in the state PQ_B^- and, following a second photoexcitation and in the absence of double reduction of Q_B, the state $PQ_A^-Q_B^-$. These results suggests that the photon induced UQ_0 semiquinone formed at Q_B does not support a photocurrent response as it cannot dissociate from the Q_B pocket [57] or transfer its electron to a second quinone in solution at an appreciable rate to permit fast RC turnover.

Finally, in optimizing an assay system for looking at the impact of quinone site mutation on photocurrent density we carried out (for the first time as far as we are aware) a systematic study of how current density depends on the type of ubiquinone used. Native ubiquinones are confined to the lipid bilayer and have an isoprenoid tail comprising 10 isoprene units (50 carbons), rendering this electron acceptor completely insoluble in an aqueous cell. As a result shorter chain analogues have been used, including UQ_2 [7,22,24,26,28,29] and UQ_0 [5,10,13,20]. Examination of ubiquinones with isoprenoid tails of varying length showed that the photocurrent density decreased with increasing numbers of isoprene units. The peak photocurrents obtained with UQ_0 and UQ_1 were identical (Fig. 5), but those obtained with UQ_2, UQ_4 and UQ_{10} dropped precipitously with increasing tail length. We have previously shown that this transient peak photocurrent is a consequence of diffusion-limited mass transport of ubiquinone from the bulk solution to the working electrode surface driven by the photocatalytic consumption of ubiquinone at the Q_B site [5]. The peak value therefore is a measure of the maximum capacity of the RC layer and associated quinones to support a current, whereas the amplitude of the later steady-state current reflects limitations arising from quinone exchange due to decreased relative solubilities of different quinones in the bulk aqueous phase. The steady-state photocurrent magnitudes were more strongly attenuated than peak photocurrents with increasing tail length, due to an increasingly lower quinone solubilities and decreased diffusion coefficients under steady turnover conditions. The clear conclusion from these assays was that the highest currents in our aqueous electrochemical cell were supported by UQ_0 as opposed to UQ_1 or, as is often used in such studies, UQ_2 [7].

4. Conclusion

In conclusion we show that electron transfer through surface-bound electrically-wired RCs is hampered by disruption of Q_A binding, Q_B binding, Q_B protonation and ubiquinone exchange. This behaviour reflects that of RCs in their native cellular environment and highlights the intact native functionality of the ubiquinone reductase mechanism of the RC in generating photocurrent. Effective adaptation of these pigment-proteins from their natural environment to that of a biohybrid device was achieved using a ubiquinone with a fully truncated isoprenoid tail, any negative impacts on binding or UQ turnover at the Q_B site being offset by the high concentration of UQ_0 that could be achieved in solution. This resulted in a peak photocurrent density of 12 μA cm-2, one of the largest photocurrents to date for a reaction center without an attendant light-harvesting system. These findings lay the groundwork for further enhancement of RC turnover and photocurrent generation via protein and/or interfacial electrode engineering to meet the demands of a viable biosensor or biophotovoltaic device.

5. Materials and methods

5.1. Experimental materials

A strain of *Rba. sphaeroides* expressing His-tagged WT RCs was constructed as described previously [10]. To construct the EL212W RC, residue Glu 212 of the L-polypeptide was changed to Trp, and to construct

the EL212A/DL213A RC residues Glu 212 and Asp 213 of this polypeptide were both changed to Ala. All mutations were introduced using the QuikChange method (Stratagene), were restricted to the target codons and were confirmed by DNA sequencing. For X-ray crystallography, mutations were introduced into plasmid pUCXB-1 which is a derivative of pUC19 containing a 1841 bp *Xba*I–*Bam*HI fragment encompassing the genes for the RC L and M polypeptides [35]. *Xba*I/*Bam*HI restriction fragments containing the mutations were shuttled into expression vector pRKEH10D [58]. For all other work, mutations were introduced into plasmid pv102, which was plasmid pUCXB-1 modified with a sequence that placed ten His residues at the C-terminus of the RC M-polypeptide [10]. XbaI/*Bam*HI restriction fragments containing the mutations were then shuttled into expression vector pv4, which is a derivative of broad-host-range vector pRK415 containing a 6.2 kb *Eco*RI–*Hin*dIII fragment encoding *pufQLM*; this vector allows expression of the RC L and M polypeptides in the absence of the α and β polypeptides of the LH1 antenna complex or the PufX polypeptide. In both cases the expression vector was introduced into *Rba. sphaeroides* deletion strain DD13 by conjugative transfer as described previously [59]. Both procedures yielded transconjugant strains that had mutant RCs but lacked both types of *Rba. sphaeroides* light-harvesting complex, and these were grown under dark/semi-aerobic conditions at 34 °C and 180 rpm in M22+ medium as described elsewhere [58]. Bacterial cells were harvested by centrifugation.

5.2. RC purification

To prepare RCs for X-ray crystallography, intracytoplasmic membranes were isolated by breakage of harvested bacterial cells in a French pressure cell and separated from cell debris and soluble components by centrifugation [60]. RCs were purified for structure determination as described in detail previously [61], the procedure employing solubilization of the RC in lauryldimethylamine oxide (LDAO) followed by three steps of anion exchange and one of gel filtration.

For RCs for photochronoamperometry, harvested bacterial cells were broken in a cell disruptor (Constant Systems) and His-tagged RCs purified by nickel affinity chromatography followed by gel filtration as described in detail recently [10].

5.3. X-ray crystallography

Engineered RCs were crystallised by sitting drop vapour diffusion [61]. Droplets contained 9 mg mL^{-1} RC, 0.09% *v*/v LDAO, 3.5% *w*/*v* 1,2,3-heptanetriol, and 0.75 M potassium phosphate (pH 7.5) and were equilibrated against a reservoir of 1.5 M potassium phosphate. Trigonal crystals with a space group of $P3_121$ grew within four weeks, were 0.5 to 2.0 mm in the longest dimension, and had approximate unit cell dimensions of a = b = 138 Å, c = 184 Å, α = β = 90°, γ = 120°.

For mounting in cryoloops, RC crystals washed in artificial mother liquor were moved sequentially through liquors with increasing concentrations of glycerol to reach a final glycerol concentration of 35%. X-ray diffraction data were collected at 100 K on a ADSC Quantum 4R CCD detector on station 14.1 of the Daresbury Synchrotron Radiation Source and processed using the HKL2000 package [62]. Collection and refinement statistics are given in Table 1. Molecular replacement was performed in AMORE [63]using the coordinates of the WT RC [61]as a starting model. This was followed by refinement using REFMAC 5 [64]. In the Figures, structures were illustrated using PyMOL [65].

5.4. Charge recombination kinetics

Charge recombination kinetics were measured using a Cary 60 spectrophotometer connected with a fiber optic coupler to an external 1 cm cuvette holder. A 50 ms flash of white light was applied at a right angle to the measuring beam from an HL-2000-FHSA halogen light source controlled by a shutter triggered by a TGP110 pulse generator (Thurlby Thandur Instruments). A mirrored insert was positioned opposite the excitation source to double the excitation light intensity, measured at 25 W m^{-2}. Solutions of reaction centers at 13.2 μM were prepared in 20 mM Tris pH 8, 200 mM NaCl, 0.1% LDAO and either 250 μM UQ_{10} or 1 mM UQ_0, and dark adapted for 1 h before measurement. A volume of 100 μL of each sample was loaded into a 3 × 3 mm florescence cuvette (Hellma). Data were collected at 865 nm with a time interval of 0.0125 s over a total period of 30 s for the WT RC and all mutants except the dAla RC, which required a measurement of 60 s to observe complete relaxation to the ground state. The flash was applied after 10 s with relaxation over the remainder of the measurement. Eight transients were measured for each protein preparation, averaged and the data were fit to either single or double exponential functions in Origin 8.0 to determine the rate constant(s). The UQ_0 concentration of 1 mM used in these experiments was the minimum required for full reconstitution of the WT RC. This was over four-fold greater than that of Q_{10}, which has a much greater affinity for the Q_B site [66] .

5.5. Fabrication of electrodes

Planar disc gold working electrodes of 2 mm diameter (CHI Instruments) were mechanically polished to a mirror-like finish using Al_2O_3 lapping films of successively finer grain sizes of 5, 3 and 1 μm (Thor Labs), followed by rinsing of the electrode with Milli-Q water after each polishing step. To form the SAM, the electrode was incubated in a solution containing 10 mM 4-mercaptopyridine (in Milli-Q water) for 10 min. Following thorough rinsing, the SAM coated gold electrodes were drop-casted with 7.5 μL of 10 μM RC complex for 30 min in the dark at 4 °C. Unbound protein was removed by controlled, repeated dipping in 20 mM Tris (pH 8) at 4 °C using a home-built dipping apparatus.

Table 1
Crystallographic statistics for data collection and refinement.

	EL212W	EL212A/DL213A/LM215A
Collection statistics		
resolution range [a]	18–2.4 Å (2.44–2.4 Å)	23.9–2.5 Å (2.56–2.5 Å)
unit cell	$a = b = 139.82$ Å, $c = 185.25$ Å $\alpha = \beta = 90°, \gamma = 120°$	$a = b = 139.0$ Å, $c = 184.7$ Å $\alpha = \beta = 90°, \gamma = 120°$
no. of reflections	307297	360990
no. of unique reflections	77800	70501
R_{merge} [b]	5.7% (50.2%)	7.2% (53.5%)
completeness	95.0% (95.6%)	98.4% (97.9%)
I/sigI	16.4 (1.63)	16.0 (2.7)
redundancy	4.2 (4.0)	5.1 (4.8)
Refinement		
resolution range	17.9–2.4	23.9–2.5
no of reflections	73853	66935
R_{factor} [c]	19.0	17.0
R_{free} [d],	21.7	19.8
RMSD bonds	0.014 Å	0.017 Å
RMSD angles	1.763 °	1.931 °
Ramachandran plot		
preferred	97.1%	97.1%
allowed	2.5%	2.78%
outliers	0.4%	0.12%
no. of amino acid residues	L: 281; M: 299; H: 238	L: 281; M: 299; H: 239
no. of non protein residues[e]	4 BChl, 2 BPheo, 2 Ubi, 1 Fe, 1 Spn, 1 Cdl, 5 LDAO, 3 Hyd, 292 waters	4 BChl, 2 BPheo, 2 Ubi, 1 Fe, 1 Spn, 1 Cdl, 3 LDAO, 5 Hyd, 302 waters, 1 phosphate

[a] Values in parentheses are for the outer resolution shell.
[b] $R_{merge} = \sum_h \sum_i |\langle I(h)\rangle - I(h)_i| / \sum_h \sum_i I(h)_i$ where $I(h)$ is the intensity of reflection h, $\sum_h$ is the sum over all reflections, and $\sum_i$ is the sum over all i measurements of reflection h.
[c] R_{factor} is defined by $\sum ||F_o| - |F_c| / \sum |F_o|$.
[d] R_{free} was calculated with 5% reflections selected to be the same as in the refinement of the WT RC [61].
[e] Abbreviations: BChl, bacteriochlorophyll; BPhe, bacteriopheophytin, Ubi, ubiquinone; Spn, spheroidenone (carotenoid); Cdl, cardiolipin; Hyd, hydrocarbon chain.

Table 2
Recombination values for RCs and RCs reconstituted in UQ_0 or UQ_{10}.

Sample	Additions	τ fast (s)	Amp fast (%)	τ slow (s)	Amp slow (%)
WT	None	0.210 ± 0.040	18 ± 2	1.21 ± 0.03	81 ± 2
dAla	None	0.108 ± 0.005	80 ± 2	22.0 ± 1.0	19.4 ± 0.4
AM260W	None	n/a[a]	n/a[a]	n/a[a]	n/a[a]
EL212W	None	0.125 ± 0.005	100 ± 2	n/a[b]	n/a[a]
WT	UQ_{10}	n/a[b]	n/a[b]	1.09 ± 0.2	100 ± 1
dAla	UQ_{10}	0.097 ± 0.009	52 ± 3	20.3 ± 0.6	47.7 ± 0.4
AM260W	UQ_{10}	n/a[a]	n/a[a]	n/a[a]	n/a[a]
EL212W	UQ_{10}	0.125 ± 0.006	100 ± 3	n/a[b]	n/a[a]
WT	UQ_0	n/a[a]	n/a[a]	1.21 ± 0.02	100 ± 1
dAla	UQ_0	0.103 ± 0.008	69 ± 3	11.4 ± 0.3	31 ± 0.4
AM260W	UQ_0	0.100 ± 0.030	52 ± 9	2.6 ± 0.2	48 ± 3
EL212W	UQ_0	0.116 ± 0.007	87 ± 3	4.4 ± 0.5	13 ± 1

[a] No photobleach observed
[b] Only one rate observed

Subsequently, coated electrodes were incubated for 5 min in a solution containing 200 μM cyt *c* in 20 mM Tris (pH 8), followed by another round of rinsing to remove unbound cyt *c*.

5.6. Photochronoamperometry

Au|4-MP|cyt *c*|RC electrodes were inserted into a photoelectrochemical cell fitted with a Ag/AgCl/3 M KCl reference electrode and a platinum counter electrode (Metrohm Autolab BV, Utrecht, Netherlands) in a working solution of 500 μM UQ_0 in 20 mM Tris (pH 8) unless stated otherwise. A PGSTAT128N potentiostat (Metrohm Autolab) was used to control the three-electrode cell, a bias potential of −68 mV vs. Ag/AgCl (−100 mV vs. SCE) being applied for all experiments. The working electrode was illuminated with an 870 nm LED ((Roithner Lasertechnik) with an irradiance of 46 mW cm^{-2} at the electrode surface. All photocurrent measurements were performed under ambient conditions, in air at room temperature.

5.7. Ubiquinone Isoprenyl tail length assays

Quinones UQ_0 and UQ_1 were solubilized in the working buffer (20 mM Tris pH 8.0) to 500 μM as determined spectroscopically. This concentration has previously been determined to be saturating for photocurrent generation with UQ_0 [10]. Quinones UQ_2, UQ_4 and UQ_{10} were solubilized to their maximum achievable concentration in the working solution, which was determined spectroscopically to be 326 μM, 3.0 μM and 0.1 μM, respectively. Solubilization of ubiquinones with detergents to achieve equimolar concentrations (as in 6.4) was not utilized as the presence of detergent in the working buffer desorbed the electrode bound RCs, resulting in further decreased photocurrent magnitudes, due to RC desorption (data not shown). An extinction coefficient of 15,100 M^{-1} cm^{-1} at 275 nm was used to determine the maximum solubility for the oxidized UQ form [67]. Photocurrent measurements were performed as described in the last section.

Table 3
Photocurrent density under 46 mW cm^{-2} irradiation (870 nm) at −68 mV vs. Ag/AgCl.

RC	j_{photo} (μA cm^{-2})	RC k_{app} (e^- s^{-1} RC $^{-1}$)	Ratio (mutant: WTRC) %
WT	12.8 ± 1.0	11.8 ± 1.23	100%
AM260W	0.4 ± 0.04	0.04 ± 0.01	3.1%
dAla	0.64 ± 0.15	0.6 ± 0.01	5.0%
EL212W	1.0 ± 0.2	0.9 ± 0.01	7.8%
RC + Stig (100 μM)	0.09 ± 0.02	0.08 ± 0.02	0.7%

Errors represent one standard deviation of uncertainty, $n = 4$.
Loading was measured at 10.9 pm cm^{-2} ± 0.8 for WT RC, and assumed identical for all mutants which were incubated under identical conditions.

5.8. Quantification of RC loading and k_{app}

Upon completion of photocurrent measurements, working electrodes were hermetically sealed in a 500 μL Eppendorf microcentrifuge tube containing 250 μL of a solution of 80% acetone and 20% Milli-Q water saturated with Na_2CO_3, then vortexed for 30 s in the dark, followed by sonication (30s). The electrode was removed and the absorbance spectrum of the solution containing extracted bacteriochlorins was then recorded. The loading of RCs on each electrode (Γ_{RC}, [mol cm^{-2}]) was estimated using an extinction coefficient at 770 nm for BChl a in 80% acetone of 69.3 ± 0.3 mM^{-1} cm^{-1} [68], and by assuming each *Rba. sphaeroides* RC complexes contains 4 molecules of BChl a. The apparent RC turnover frequency (k_{app}) was determined using:

$$k_{app} = \frac{j_{photo}}{n\Gamma F}$$

where j_{photo} is the photocurrent flux in A cm^{-2}, Γ is the RC loading in mol cm^{-2}, *F* is Faraday's constant (96,485 C mol^{-1}) and n is the number of electrons per turnover (one in this case). The turnover rates reported are an apparent value because we assume all bound RCs are assumed to be active in photocurrent generation.

Author contributions

D.J.K.S., P.K.F. and M.R.J. provided purified WT and engineered RC complexes. V.M.F. & D.J.K·S performed photochronoamperometry. P.K.F. performed X-ray crystallography. W.v.d.H. performed photoelectrochemical experiments with UQ mediators. D.J.K.S. performed spectroscopic single turnover flash measurements and analysis. V.M.F., D.J.K.S, P.K.F, J.D.D., M.R.J. and R.N.F. wrote the manuscript. All authors discussed the results and commented on the manuscript.

Competing financial interests

The authors state no competing financial interest.

Transparency document

The Transparency document associated with this article can be found, in online version.

Acknowledgements

M.R.J., P.K.F and D.J.K.S. acknowledge support from the Biotechnology and Biological Sciences Research Council of the UK (projects B13439 and BB/I022570/1). R.N.F. acknowledges support from the Dutch science foundation NWO for a vidi grant, D.M. for a veni grant (no.

722.011.003). M.R.J., R.N.F., D.J.K.S., V.M.F. and J.D.D. acknowledge support via EU COST Action TD1102 — Photosynthetic proteins for technological applications: biosensors and biochips (PHOTOTECH).

References

[1] C.A. Wraight, R.K. Clayton, The absolute quantum efficiency of bacteriochlorophyll photooxidation in reaction centres of Rhodopseudomonas spheroides, Biochim. Biophys. Acta - Bioenerg. 333 (1974) 246–260, http://dx.doi.org/10.1016/0005-2728(74)90009-7.

[2] P. Heathcote, M. Jones, 8.7 the structure-function relationships of photosynthetic reaction centers, Compr. Biophys, https://scholar.google.nl/scholar?cluster=4736545226534781105&hl=en&as_sdt=5,41&sciodt=0,41#0 2012 (accessed May 7, 2016).

[3] N. Nelson, C.F. Yocum, Structure and function of photosystems I and II, Annu. Rev. Plant Biol. 57 (2006) 521–565, http://dx.doi.org/10.1146/annurev.arplant.57.032905.105350.

[4] S.M. Mirvakili, J.E. Slota, A.R. Usgaocar, A. Mahmoudzadeh, D. Jun, M.N. Mirvakili, J.T. Beatty, J.D.W. Madden, Photoactive electrodes incorporating electrosprayed bacterial reaction centers, Adv. Funct. Mater. 24 (2014) 4789–4794, http://dx.doi.org/10.1002/adfm.201400350.

[5] V.M. Friebe, J.D. Delgado, D.J.K. Swainsbury, J.M. Gruber, A. Chanaewa, R. van Grondelle, E. von Hauff, D. Millo, M.R. Jones, R.N. Frese, Plasmon-enhanced photocurrent of photosynthetic pigment proteins on nanoporous silver, Adv. Funct. Mater. (2015), http://dx.doi.org/10.1002/adfm.201504020 (n/a–n/a).

[6] S.C. Tan, S.K. Ravi, Progress and perspectives in exploiting photosynthetic biomolecules for solar energy harnessing, Energy Environ. Sci. (2015), http://dx.doi.org/10.1039/C5EE01361E.

[7] H. Yaghoubi, E. Lafalce, D. Jun, X. Jiang, J.T. Beatty, A. Takshi, Large photocurrent response and external quantum efficiency in biophotoelectrochemical cells incorporating reaction center plus light harvesting complexes, Biomacromolecules 16 (2015) 1112–1118, http://dx.doi.org/10.1021/bm501772x.

[8] S.C. Tan, L.I. Crouch, M.R. Jones, M. Welland, Generation of alternating current in response to discontinuous illumination by photoelectrochemical cells based on photosynthetic proteins, Angew. Chem. Int. Ed. Engl. 51 (2012) 6667–6671, http://dx.doi.org/10.1002/anie.201200466.

[9] T. Kothe, N. Plumeré, A. Badura, M.M. Nowaczyk, D.a. Guschin, M. Rögner, W. Schuhmann, Combination of a photosystem 1-based photocathode and a photosystem 2-based photoanode to a z-scheme mimic for biophotovoltaic applications, Angew. Chem. Int. Ed. 52 (2013) 14233–14236, http://dx.doi.org/10.1002/anie.201303671.

[10] D.J.K. Swainsbury, V.M. Friebe, R.N. Frese, M.R. Jones, Evaluation of a biohybrid photoelectrochemical cell employing the purple bacterial reaction Centre as a biosensor for herbicides, Biosens. Bioelectron. 58 (2014) 172–178, http://dx.doi.org/10.1016/j.bios.2014.02.050.

[11] M. Chatzipetrou, F. Milano, L. Giotta, D. Chirizzi, M. Trotta, M. Massaouti, M.R. Guascito, I. Zergioti, Functionalization of gold screen printed electrodes with bacterial photosynthetic reaction centers by laser printing technology for mediatorless herbicide biosensing, Electrochem. Commun. 64 (2016) 46–50, http://dx.doi.org/10.1016/j.elecom.2016.01.008.

[12] B.D. Reiss, D.K. Hanson, M.A. Firestone, Evaluation of the photosynthetic reaction center protein for potential use as a bioelectronic circuit element, Biotechnol. Prog. 23 985–9, http://dx.doi.org/10.1021/bp070042s.

[13] M. Kamran, V.M. Friebe, J.D. Delgado, T.J. Aartsma, R.N. Frese, M.R. Jones, Demonstration of asymmetric electron conduction in pseudosymmetrical photosynthetic reaction centre proteins in an electrical circuit, Nat. Commun. 6 (2015) 6530, http://dx.doi.org/10.1038/ncomms7530.

[14] A.F. Janzen, M. Seibert, Photoelectrochemical conversion using reaction-centre electrodes, Nature 286 (1980) 584–585, http://dx.doi.org/10.1038/286584a0.

[15] G. LeBlanc, E. Gizzie, S. Yang, D.E. Cliffel, G.K. Jennings, Photosystem I protein films at electrode surfaces for solar energy conversion, Langmuir (2014).

[16] O. Yehezkeli, R. Tel-Vered, D. Michaeli, I. Willner, R. Nechushtai, Photosynthetic reaction center-functionalized electrodes for photo-bioelectrochemical cells, Photosynth. Res. 120 (2014) 71–85, http://dx.doi.org/10.1007/s11120-013-9796-3.

[17] A. Mershin, K. Matsumoto, L. Kaiser, D. Yu, M. Vaughn, M.K. Nazeeruddin, B.D. Bruce, M. Graetzel, S. Zhang, Self-assembled photosystem-I biophotovoltaics on nanostructured TiO(2)and ZnO, Sci. Rep. 2 (2012) 234, http://dx.doi.org/10.1038/srep00234.

[18] H. Yaghoubi, Z. Li, D. Jun, E. Lafalce, X. Jiang, R. Schlaf, J.T. Beatty, A. Takshi, Hybrid wiring of the Rhodobacter sphaeroides reaction center for applications in biophotoelectrochemical solar cells, J. Phys. Chem. C 118 (2014) 23509–23518, http://dx.doi.org/10.1021/jp507065u.

[19] M. Kamran, J.D. Delgado, V. Friebe, T.J. Aartsma, R.N. Frese, Photosynthetic protein complexes as bio-photovoltaic building blocks retaining a high internal quantum efficiency, Biomacromolecules 15 (2014) 2833–2838, http://dx.doi.org/10.1021/bm500585s.

[20] M.-J. den Hollander, J.G. Magis, P. Fuchsenberger, T.J. Aartsma, M.R. Jones, R.N. Frese, Enhanced photocurrent generation by photosynthetic bacterial reaction centers through molecular relays, light-harvesting complexes, and direct protein–gold interactions, Langmuir 27 (2011) 10282–10294, http://dx.doi.org/10.1021/la2013528.

[21] R. Das, P.J. Kiley, M. Segal, J. Norville, a.A. Yu, L. Wang, S.a. Trammell, L.E. Reddick, R. Kumar, F. Stellacci, N. Lebedev, J. Schnur, B.D. Bruce, S. Zhang, M. Baldo, Integration of photosynthetic protein molecular complexes in solid-state electronic devices, Nano Lett. 4 (2004) 1079–1083, http://dx.doi.org/10.1021/nl049579f.

[22] S.a. Trammell, L. Wang, J.M. Zullo, R. Shashidhar, N. Lebedev, Orientated binding of photosynthetic reaction centers on gold using Ni-NTA self-assembled monolayers, Biosens. Bioelectron. 19 (2004) 1649–1655, http://dx.doi.org/10.1016/j.bios.2003.12.034.

[23] S.C. Tan, L.I. Crouch, S. Mahajan, M.R. Jones, M.E. Welland, Increasing the open-circuit voltage of photoprotein-based photoelectrochemical cells by manipulation of the vacuum potential of the electrolytes, ACS Nano 6 (2012) 9103–9109, http://dx.doi.org/10.1021/nn303333e.

[24] M. Kondo, Y. Nakamura, K. Fujii, M. Nagata, Y. Suemori, T. Dewa, K. Iida, A.T. Gardiner, R.J. Cogdell, M. Nango, Self-assembled monolayer of light-harvesting core complexes from photosynthetic bacteria on a gold electrode modified with alkanethiols, Biomacromolecules 8 (2007) 2457–2463, http://dx.doi.org/10.1021/bm070352z.

[25] G. Leblanc, G. Chen, E.A. Gizzie, G.K. Jennings, D.E. Cliffel, Enhanced photocurrents of photosystem I films on p-doped silicon, Adv. Mater. (2012) http://dx.doi.org/10.1002/adma.201202794.

[26] H. Yaghoubi, Z. Li, D. Jun, E. Lafalce, X. Jiang, R. Schlaf, J.T. Beatty, A. Takshi, Hybrid wiring of the Rhodobacter sphaeroides reaction Center for Applications in biophotoelectrochemical solar cells, J. Phys. Chem. C 118 (2014) 23509–23518, http://dx.doi.org/10.1021/jp507065u.

[27] N. Lebedev, S.A. Trammell, A. Spano, E. Lukashev, I. Griva, J. Schnur, Conductive wiring of immobilized photosynthetic reaction center to electrode by cytochrome *c*, J. Am. Chem. Soc. 128 (2006) 12044–12045, http://dx.doi.org/10.1021/ja063367y.

[28] N. Lebedev, S.A. Trammell, S. Tsoi, A. Spano, J.H. Kim, J. Xu, M.E. Twigg, J.M. Schnur, Increasing efficiency of photoelectronic conversion by encapsulation of photosynthetic reaction center proteins in arrayed carbon nanotube electrode, Langmuir 24 (2008) 8871–8876, http://dx.doi.org/10.1021/la8011348.

[29] S.A. Trammell, I. Griva, A. Spano, S. Tsoi, L.M. Tender, J. Schnur, N. Lebedev, Effects of distance and driving force on photoinduced electron transfer between photosynthetic reaction centers and gold electrodes, J. Phys. Chem. C 111 (2007) 17122–17130, http://dx.doi.org/10.1021/jp0740402.

[30] W. Zinth, J. Wachtveitl, The first picoseconds in bacterial photosynthesis–ultrafast electron transfer for the efficient conversion of light energy, ChemPhysChem 6 (2005) 871–880, http://dx.doi.org/10.1002/cphc.200400458.

[31] E. Takahashi, C.A. Wraight, Proton and electron transfer in the acceptor quinone complex of Rhodobacter sphaeroides reaction centers: characterization of site-directed mutants of the two ionizable residues, GluL212 and AspL213, in the QB binding site, Biochemistry 31 (1992) 855–866, http://dx.doi.org/10.1021/bi00118a031.

[32] M. Okamura, M. Paddock, M. Graige, G. Feher, Proton and electron transfer in bacterial reaction centers, Biochim. Biophys. Acta - Bioenerg. 1458 (2000) 148–163, http://dx.doi.org/10.1016/S0005-2728(00)00065-7.

[33] M.L. Paddock, P.H. McPherson, G. Feher, M.Y. Okamura, Pathway of proton transfer in bacterial reaction centers: replacement of serine-L223 by alanine inhibits electron and proton transfers associated with reduction of quinone to dihydroquinone, Proc. Natl. Acad. Sci. U. S. A. 87 (1990) 6803–6807, http://dx.doi.org/10.1073/pnas.87.17.6803.

[34] P.K. Fyfe, J.A. Potter, J. Cheng, C.M. Williams, A.J. Watson, M.R. Jones, Structural responses to cavity-creating mutations in an integral membrane protein, Biochemistry 46 (2007) 10461–10472, http://dx.doi.org/10.1021/bi701085w.

[35] J.P. Ridge, M.E. Van Brederode, M.G. Goodwin, R. Van Grondelle, M.R. Jones, Mutations that modify or exclude binding of the Q(A) ubiquinone and carotenoid in the reaction center from Rhodobacter sphaeroides, Photosynth. Res. 59 (1999) 9–26, http://dx.doi.org/10.1023/A:1006111321083.

[36] K.E. McAuley, P.K. Fyfe, J.P. Ridge, R.J. Cogdell, N.W. Isaacs, M.R. Jones, Ubiquinone binding, ubiquinone exclusion, and detailed cofactor conformation in a mutant bacterial reaction center †, Biochemistry 39 (2000) 15032–15043, http://dx.doi.org/10.1021/bi000557r.

[37] D.K. Hanson, L. Baciou, D.M. Tiede, S.L. Nance, M. Schiffer, P. Sebban, In bacterial reaction centers protons can diffuse to the secondary quinone by alternative pathways, Biochim. Biophys. Acta - Bioenerg. 1102 (1992) 260–265, http://dx.doi.org/10.1016/0005-2728(92)90108-E.

[38] D.K. Hanson, S.L. Nance, M. Schiffer, Second-site mutation at M43 (Asn?Asp) compensates for the loss of two acidic residues in the QB site of the reaction center, Photosynth. Res. 32 (1992) 147–153, http://dx.doi.org/10.1007/BF00035949.

[39] D.K. Hanson, D.M. Tiede, S.L. Nance, C.H. Chang, M. Schiffer, Site-specific and compensatory mutations imply unexpected pathways for proton delivery to the QB binding site of the photosynthetic reaction center, Proc. Natl. Acad. Sci. U. S. A. 90 (1993) 8929–8933 http://www.pubmedcentral.nih.gov/articlerender.fcgi?artid=47474&tool=pmcentrez&rendertype=abstract accessed November 11, 2015.

[40] P.R. Pokkuluri, P.D. Laible, Y.-L. Deng, T.N. Wong, D.K. Hanson, M. Schiffer, The structure of a mutant photosynthetic reaction center shows unexpected changes in main chain orientations and quinone position, Biochemistry 41 (2002) 5998–6007, http://dx.doi.org/10.1021/bi0118963.

[41] A. Wraight, Colin, proton and electron transfer in the acceptor quinone complex of photosynthetic reaction centers from Rhodobacter sphaeroides, Front. Biosci. 9 (2004) 309, http://dx.doi.org/10.2741/1236.

[42] E. Nabedryk, J. Breton, Coupling of electron transfer to proton uptake at the Q(B) site of the bacterial reaction center: a perspective from FTIR difference spectroscopy, Biochim. Biophys. Acta 1777 (2008) 1229–1248, http://dx.doi.org/10.1016/j.bbabio.2008.06.012.

[43] D. Kleinfeld, M.Y. Okamura, G. Feher, Electron transfer in reaction centers of Rhodopseudomonas sphaeroides. I. Determination of the charge recombination pathway of D + QAQ − B and free energy and kinetic relations between Q − AQB and QAQ − B, Biochim. Biophys. Acta - Bioenerg. 766 (1984) 126–140, http://dx.doi.org/10.1016/0005-2728(84)90224-X.

[44] D. Frolov, M.C. Wakeham, E.G. Andrizhiyevskaya, M.R. Jones, R. van Grondelle, Investigation of B-branch electron transfer by femtosecond time resolved spectroscopy in a Rhodobacter sphaeroides reaction centre that lacks the Q(A) ubiquinone, Biochim. Biophys. Acta 1707 (2005) 189–198, http://dx.doi.org/10.1016/j.bbabio.2004.12.006.
[45] J. Breton, M.C. Wakeham, P.K. Fyfe, M.R. Jones, E. Nabedryk, Characterization of the bonding interactions of Q(B) upon photoreduction via A-branch or B-branch electron transfer in mutant reaction centers from Rhodobacter sphaeroides, Biochim. Biophys. Acta 1656 (2004) 127–138, http://dx.doi.org/10.1016/j.bbabio.2004.02.005.
[46] S. Monari, G. Battistuzzi, M. Borsari, D. Millo, C. Gooijer, G. Zwan, A. Ranieri, M. Sola, Thermodynamic and kinetic aspects of the electron transfer reaction of bovine cytochrome *c* immobilized on 4-mercaptopyridine and 11-mercapto-1-undecanoic acid films, J. Appl. Electrochem. 38 (2008) 885–891, http://dx.doi.org/10.1007/s10800-008-9493-7.
[47] D. Millo, A. Ranieri, P. Gross, H.K. Ly, M. Borsari, P. Hildebrandt, G.J.L. Wuite, C. Gooijer, G. van der Zwan, Electrochemical response of cytochrome c immobilized on smooth and roughened silver and gold surfaces chemically modified with 11-Mercaptounodecanoic acid, J. Phys. Chem. C 113 (2009) 2861–2866, http://dx.doi.org/10.1021/jp807855y.
[48] K. Warncke, M.R. Gunner, B.S. Braun, L. Gu, C.a. Yu, J.M. Bruce, P.L. Dutton, Influence of hydrocarbon tail structure on quinone binding and electron-transfer performance at the QA and QB sites of the photosynthetic reaction center protein, Biochemistry 33 (1994) 7830–7841, http://dx.doi.org/10.1021/bi00191a010.
[49] G. von Jagow, T. Ohnishi, The chromone inhibitor stigmatellin - binding to the ubiquinol oxidation center at the C-side of the mitochondrial membrane, FEBS Lett. 185 (1985) 311–315, http://dx.doi.org/10.1016/0014-5793(85)80929-7.
[50] N.P. Pawlowicz, R. van Grondelle, I.H.M. van Stokkum, J. Breton, M.R. Jones, M.L. Groot, Identification of the first steps in charge separation in bacterial photosynthetic reaction centers of Rhodobacter sphaeroides by ultrafast mid-infrared spectroscopy: electron transfer and protein dynamics, Biophys. J. 95 (2008) 1268–1284, http://dx.doi.org/10.1529/biophysj.108.130880.
[51] K. Gibasiewicz, M. Pajzderska, A. Dobek, J. Karolczak, G. Burdziński, K. Brettel, M.R. Jones, Analysis of the temperature-dependence of P(+)HA(−) charge recombination in the Rhodobacter sphaeroides reaction center suggests nanosecond temperature-independent protein relaxation, Phys. Chem. Chem. Phys. 15 (2013) 16321–16333, http://dx.doi.org/10.1039/c3cp44187c.
[52] M.C. Wakeham, J. Breton, E. Nabedryk, M.R. Jones, Formation of a semiquinone at the QB site by A- or B-branch electron transfer in the reaction center from Rhodobacter sphaeroides, Biochemistry 43 (2004) 4755–4763, http://dx.doi.org/10.1021/bi035726x.
[53] M.C. Wakeham, M.G. Goodwin, C. McKibbin, M.R. Jones, Photo-accumulation of the P+QB- radical pair state in purple bacterial reaction centres that lack the QA ubiquinone, FEBS Lett. 540 (2003) 234–240 http://www.ncbi.nlm.nih.gov/pubmed/12681514 (accessed November 11, 2015).
[54] M.L. Paddock, C. Chang, Q. Xu, E.C. Abresch, H.L. Axelrod, G. Feher, M.Y. Okamura, Quinone (QB) reduction by B-branch electron transfer in mutant bacterial reaction centers from Rhodobacter sphaeroides: quantum efficiency and X-ray structure, Biochemistry 44 (2005) 6920–6928, http://dx.doi.org/10.1021/bi047559m.
[55] A. Marchanka, A. Savitsky, W. Lubitz, K. Möbius, M. van Gastel, B-branch electron transfer in the photosynthetic reaction center of a Rhodobacter sphaeroides quadruple mutant. Q- and W-band electron paramagnetic resonance studies of triplet and radical-pair cofactor states, J. Phys. Chem. B 114 (2010) 14364–14372, http://dx.doi.org/10.1021/jp1003424.
[56] C.A. Wraight, Chance and design—proton transfer in water, channels and bioenergetic proteins, Biochim. Biophys. Acta - Bioenerg. 1757 (2006) 886–912, http://dx.doi.org/10.1016/j.bbabio.2006.06.017.
[57] B.A. Diner, C.C. Schenck, C. De Vitry, Effect of inhibitors, redox state and isoprenoid chain length on the affinity of ubiquinone for the secondary acceptor binding site in the reaction centers of photosynthetic bacteria, Biochim. Biophys. Acta - Bioenerg. 766 (1984) 9–20, http://dx.doi.org/10.1016/0005-2728(84)90211-1.
[58] M.R. Jones, R.W. Visschers, R. Van Grondelle, C.N. Hunter, Construction and characterization of a mutant of Rhodobacter sphaeroides with the reaction center as the sole pigment-protein complex, Biochemistry 31 (1992) 4458–4465, http://dx.doi.org/10.1021/bi00133a011.
[59] M.R. Jones, G.J. Fowler, L.C. Gibson, G.G. Grief, J.D. Olsen, W. Crielaard, C.N. Hunter, Mutants of Rhodobacter sphaeroides lacking one or more pigment-protein complexes and complementation with reaction-Centre, LH1, and LH2 genes, Mol. Microbiol. 6 (1992) 1173–1184.
[60] M.R. Jones, M. Heer-Dawson, T.A. Mattioli, C.N. Hunter, B. Robert, Site-specific mutagenesis of the reaction centre from Rhodobacter sphaeroides studied by Fourier transform Raman spectroscopy: mutations at tyrosine M210 do not affect the electronic structure of the primary donor, FEBS Lett. 339 (1994) 18–24 http://www.ncbi.nlm.nih.gov/pubmed/8313970 (accessed June 30, 2015).
[61] K.E. McAuley-Hecht, P.K. Fyfe, J.P. Ridge, S.M. Prince, C.N. Hunter, N.W. Isaacs, R.J. Cogdell, M.R. Jones, Structural studies of wild-type and mutant reaction centers from an antenna-deficient strain of Rhodobacter sphaeroides: monitoring the optical properties of the complex from bacterial cell to crystal, Biochemistry 37 (1998) 4740–4750, http://dx.doi.org/10.1021/bi971717a.
[62] Z. Otwinowski, W. Minor, [20] Processing of X-ray diffraction data collected in oscillation mode, Methods Enzymol. 276 (1997) 307–326, http://dx.doi.org/10.1016/S0076-6879(97)76066-X.
[63] J. Navaza, E. Vernoslova, On the fast translation functions for molecular replacement, Acta Crystallogr. Sect. A Found. Crystallogr. 51 (1995) 445–449, http://dx.doi.org/10.1107/S0108767394011335.
[64] G.N. Murshudov, A.A. Vagin, E.J. Dodson, Refinement of macromolecular structures by the maximum-likelihood method, Acta Crystallogr. Sect. D Biol. Crystallogr. 53 (1997) 240–255, http://dx.doi.org/10.1107/S0907444996012255.
[65] W. Delano, W.L. DeLano, The PyMOL Molecular Graphics System, DeLano Scientific, San Carlos (CA), USA, 2002 (Available from http://www.pymol.org., PyMOL Mol. Graph. Syst. San Carlos (CA), USA DeLano Sci. 2002. Available from Http// Www.pymol.org. (2002)).
[66] J.C. McComb, R.R. Stein, C.a. Wraight, Investigations on the influence of headgroup substitution and isoprene side-chain length in the function of primary and secondary quinones of bacterial reaction centers, Biochim. Biophys. Acta. 1015 (1990) 156–171, http://dx.doi.org/10.1016/0005–2728(90)90227-U.
[67] I. Al-Nuri, K. Rahawi, N. Sharif, UV-derivative spectra of Co-enzyme Q0. Determination of trace amounts, Iraqi Nation J. Chem. 43 (2011) 424–435 http://www.uobabylon.edu.iq/publications/chemistry_edition27/njc27_publication_14.doc (accessed May 24, 2016).
[68] H.P. Permentier, K.A. Schmidt, M. Kobayashi, M. Akiyama, C. Hager-Braun, S. Neerken, M. Miller, J. Amesz, Composition and optical properties of reaction centre core complexes from the green sulfur bacteria Prosthecochloris aestuarii and Chlorobium tepidum, Photosynth. Res. 64 (2000) 27–39, http://dx.doi.org/10.1023/A:1026515027824.